ACS MATERIALS LETTERS

www.acsmaterialsletters.org

LETTER

Flexible and Transparent High-Dielectric-Constant Polymer Films Based on Molecular Ferroelectric-Modified Poly(Vinyl Alcohol)

Yunyun Yang,[‡] Yusen Zhao,[‡] Jun Liu, Zekun Nie, Jun Ma, Mutian Hua, Yucheng Zhang, Xufu Cai,* and Ximin He*

Cite This: *ACS Materials Lett.* 2020, 2, 453−460

Read Online

ACCESS | Metrics & More | Article Recommendations | Supporting Information

ABSTRACT: Organic ferroelectrics with high dielectric constant have received substantial attention for sustainable and flexible energy storage. Here, we report a high-κ dielectric, optically transparent, mechanically strong and flexible dielectric polymer produced by in situ formation of biaxial ferroelectric-molecule-modified poly(vinyl alcohol) (PVA). The composite film was fabricated by solution casting of a PVA solution containing water-soluble dielectric crystals [Hdabco]ClO_4. Atomic force microscopic and polarized optical microscopic studies showed a uniform dispersion of TEDA.C crystals with tunable rod-like or dendritic microstructures in the PVA matrix. Because of the good compatibility and hydrogen bonds between PVA and TDEA.C, the modified PVA films presented a significant enhancement of the dielectric constant and energy storage density by 10−100-fold over neat PVA. The polarization-electric loops indicated that the PVA composite films possessed increased saturation polarization in comparison to neat PVA film. The remnant polarization of PVA composite films was improved by around 3200 times with 9 wt % TEDA.C. Also, the TEDA.C@PVA films exhibited 85% transparency throughout the visible spectrum, 116% increase in storage modulus, and 274% elongation at fracture. These unprecedented high-κ dielectric, optical, and mechanical properties may break the restrictions in the applications of traditional ferroelectric materials and greatly expand the usage of dielectric polymers in broad fields.

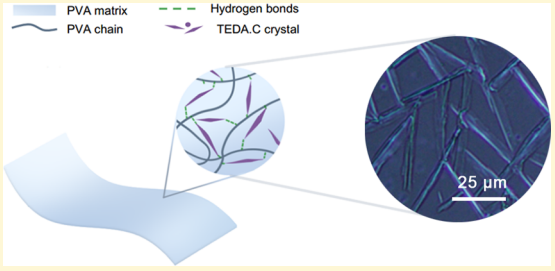

With the increasing demands of energy, exhaustion of nonrenewable fossil fuels has become one of the most pressing issues on earth.[1−4] Although various ways to harvest energy from sustainable energy sources (solar, wind, tide, etc.) have been invented, the majority of transduced energy is lost during handling, transporting, and storage, which heavily limits the application of these technologies. Therefore, efficient, sustainable, and environmentally friendly pathways to prepare energy-storage materials are urgently needed.[5−7] Dielectric capacitors with high dielectric constant and high energy storage density have drawn increasing attention as a simple and efficient method for rapid storage and release of energy.[8,9] Among them, soft polymers have become the attractive materials for next-generation dielectric capacitors owing to the flexibility, ultra-high breakdown strength, ultra-low dielectric loss, lightweight, easy processing, and cost-effectiveness. However, their low permittivity limits their applications on dielectric capacitors,[10] dielectric actuators,[11−15] and flexible electronic devices.[16]

To improve the permittivity, people have been incorporating high dielectric constant inorganic materials or conducting materials in polymer matrices, such as ferroelectric materials, semiconductors, metals, and carbon nanomaterials.[17−21] Among those additives, the ferroelectric materials, with spontaneous electric polarization, which can be reversed by external electric field, have captured broad interests because of their high dielectric constants.[22−24] To date, the majority of the commercial ferroelectrics are inorganic perovskite oxides, such as barium titanate and lead zirconate titanate.[25,26] However, these materials contain heavy-metal elements and require costly thermal and vacuum processing during preparation.[27] In addition, the large loading of fillers may cause aggregation, structural defects, and reduction of transparency and flexibility of the polymer composites materials, which will reduce the optical and mechanical performance of those composite polymer materials.[28] Mean-

Received: March 5, 2020
Accepted: March 27, 2020
Published: March 27, 2020

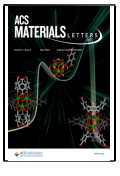

https://dx.doi.org/10.1021/acsmaterialslett.0c00086
ACS Materials Lett. 2020, 2, 453−460

while, soft electronics have emerged with the attractive properties of being highly integrated, lightweight, portable, wearable, and implantable.[29−31] Flexible polymers with high dielectric constants have been considered as ideal dielectric materials to store electric energy.[31−33] Among them, organic molecular ferroelectrics have been extensively studied to overcome the drawbacks of some commercial ferroelectrics,[34] exhibiting large spontaneous polarization (20 $\mu C/cm^2$) for croconic acid[35] and high Curie temperature (426 K).[36] According to the work of Tang et al.,[37] a biaxial molecular ferroelectric, [Hdabco]ClO_4 (dabco = diazabicyclo[2.2.2]-octane) (Figure S1), could be prepared by an environment-friendly approach and showed ultrafast polarization switching ability under high-frequency and high-temperature conditions However, the intrinsic rigid and brittle properties of TEDA.C limit its application on stretchable and flexible devices.

In this work, we successfully developed a new class of transparent and stretchable high-dielectric-constant composite polymer films by in situ embedding biaxial molecular ferroelectrics TEDA.C in PVA films. PVA was selected as the host matrix because of its high dielectric strength,[38] high mechanical strength, excellent transparency, water-solubility,[39] and dopant-dependent electrical conductivity.[40−42] The TEDA.C displayed uniform distribution in PVA films as observed by AFM and POM. PVA served as a decent protective matrix for TEDA.C because of the hydrogen bonds between TEDA.C and PVA interface. The as-formed films showed over 85% optical transparency in the visible-light region and high mechanical strength while maintaining stretchability up to 274%. Because of the strong ferroelectric property of TEDA.C, the α-relaxation of PVA and the micro-Brownian motion of long chain segments in the amorphous regions of PVA,[43,44] the conductivity of the composite film was notably increased by 3 orders of magnitude by doping 9 wt % TEDA.C. The dielectric constant was up to 10^4, which was 10−100-fold over that of neat PVA, comparable to inorganic perovskite oxide- or conductive material-modified polymer composites,[17−21] and superior to state-of-the-art dielectric PVA systems in previous reports.[45−48] The polarization-electric loops indicated that PVA composite films possessed increase in remnant polarization by around 3200 times. The high dielectric constant, stretchability and optical transparency of TEDA.C@PVA composites have potential on multifunctional electroactive application[14] with low applied voltage for soft-robotics,[11,12] optics,[15] and microfluidics.[13]

First, we synthesized the TEDA.C and characterized the chemical structures (Figures S2 and S3), crystallization properties (Figure S4), microscopic morphologies (Figures S5 and S6), optical properties (Figure S7), thermal properties (Figures S8−10), and dielectric properties (Figures S11−S19). To form the composite films for dielectric applications, we utilized solution casting after which The TEDA.C and PVA were crystallized upon evaporation of water (Figure 1A). The interaction of TEDA.C crystals with polymer chains and the charge accumulation at the interfaces between the TEDA.C crystals and the PVA chains were depicted in Figure 1B. In addition to using PVA as host materials, polypropylene (PP) and polyvinylidene fluoride (PVDF) were used to form uniform samples by melt processing and solution coating. Their results (Figures S20 and S21) indicated TEDA.C cannot improve the dielectric properties of PP and PVDF without the interaction of TEDA.C and hydroxyl groups. The mutual dissolution of TEDA.C in PVA allowed needle-like crystals to

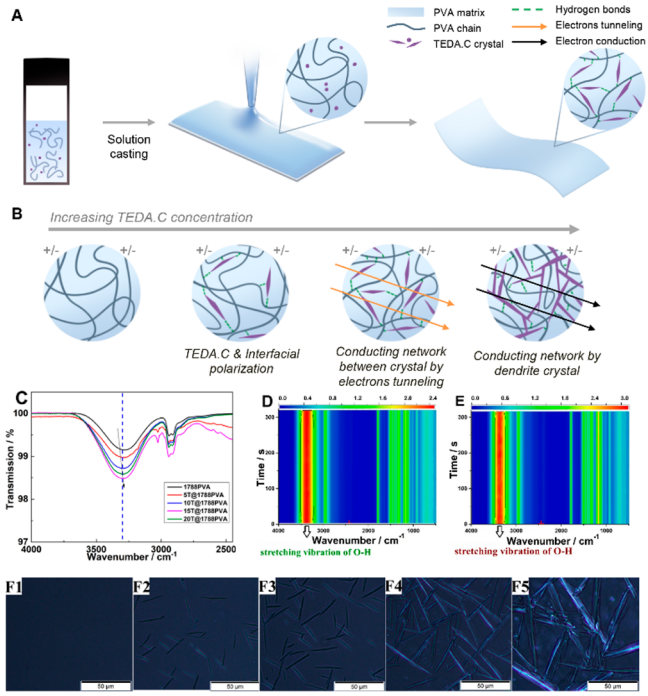

Figure 1. (A) Schematics of the preparation of TEDA.C@PVA films. (B) Mechanism of TEDA.C@PVA films: the formation of conducting networks, hydrogen bonding, and the interfacial charge accumulation contribute to the dielectric property. (C) ATR spectrum of PVA composite films (5T@1788PVA: the weight ratio of TEDA.C and 1788PVA was 5:100). (D) FTIR spectrum (with 34 scans) of 1788PVA (33 μm) films under 0.1 Hz, 0.95 V/mm AC electric field. (E) FTIR spectrum (with 34 scans) of 5T@1788PVA films (33 μm) under 0.1 Hz, 0.95 V/mm AC electric field. (F) POM images of 1788PVA, 5T@1788PVA, 10T@1788PVA, 15T@1788PVA, and 20T@1788PVA.

be uniformly dispersed in PVA matrix (Figure 1F). Furthermore, the ultrafast polarization switching of TEDA.C greatly improved the dielectric constant of the PVA composite under AC electric field. In addition, another factor was the MWS interfacial polarization.[49,50] Here, the interfacial polarization via MWS effect was increased with the increasing TEDA.C crystal impregnation into the PVA. Additionally, the interparticle distances between the TEDA.C decreased and some cross-links between TEDA.C crystals appeared with the increment of doping content. With 13 wt % addition of TEDA.C, the gradual crosslinking of crystals formed a dendritic crystal network within PVA matrix, which can act as conducting network and increase the dielectric constant.

The hydrogen bonds between negative charges on the crystal surface (N) and H atoms on the polymer backbone can form a dipole that responds to the applied electric field. Previous reports have demonstrated that large dipole moment of such hydrogen bonds can be the key factor for dielectric constant enhancement of a PVDF/hydrated metal salt composite[51] and PVDF/MXene.[18] We also investigated the change in bond strength between −OH bonds in PVA by Attenuated total reflection (ATR) (Figure 1C). With the increased concentration of TEDA.C, the peak of −OH blue-shifted and the transmission of −OH decreased, indicating more hydrogen bonds formed in the film. Figure 1D and Figure 1E showed the Fourier-transform infrared spectrum (FTIR) of films under AC electric field (the 3D views of FTIR

https://dx.doi.org/10.1021/acsmaterialslett.0c00086
ACS Materials Lett. 2020, 2, 453−460

spectrum are shown in Figure S22). To avoid the effect of film transparency on the absorption of infrared spectrum, low addition of TEDA.C composites films were chosen for this measurement. The region of 3600−3000 cm^{-1} corresponded to the stretching vibration of O−H groups. The absorbance of 1788PVA was about 80% of that of 5T@1788PVA. Notably, changes in the absorbance strength of 5T@1788PVA occurred under AC electric field, suggesting the dipole moment of hydrogen bonds formed by charges accumulation at composite interfaces under AC electric field. The POM images showed that 1788PVA was contrast-less and homogeneous owing to the amorphous structure of poly(vinyl alcohol) (Figure 1F). The addition of TEDA.C led to the formation of rod-like crystals. With the increasing concentration of TEDA.C, the length and diameter of the crystals also increased. When the addition of TEDA.C was above 9 wt %, dendritic crystals with crosslinked network began to form.

Figure 2 listed the frequency-dependent, temperature-dependent dielectric constants and dielectric loss. The results showed that, with low addition (4.7, 9, and 13 wt %) of TEDA.C, the dielectric constant of PVA composites increased by 10−50 times over the entire tested frequency range from 10 Hz to 1 MHz. This pronounced increase in the dielectric constant of composite films can be attributed to the strong ferroelectric property of TEDA.C, which comes from the chemical nature of the material (Figures S11−13 and S16−S18).[37] For the composite with 16 wt % TEDA.C, its dielectric constant grew exponentially with decreasing frequency. The ε' of 33356.9 obtained at 0.1 Hz was 6271.2 times of 1788PVA without TEDA.C at room temperature (Figure 2A1, the same comparison at 383 K was showed in Figure S23). The increment was due to the Maxwell−Wagner−Sillars interfacial polarization occurred at the interfaces between the TEDA.C and PVA chains, which typically appeared within a heterogeneous system of phases with nonidentical conductivity via accumulation of charges at the interfacial surfaces.[49,50] To the best of our knowledge, the dielectric constant increase demonstrated in this work were higher than previous works, as summarized in Table 1. Meanwhile, the film can maintain a low dielectric loss with slightly lower addition of TEDA.C before 10 Hz as shown in Figure 2B1. The dielectric losses of the 5T@1788PVA (the weight ratio of TEDA.C and 1788PVA was 5:100), 10T@1788PVA, 15 T@1788PVA thin films were lower than that of 1788PVA at low frequency, which may be due to the polarization effects and dipoles of TEDA.C. The temperature-dependent dielectric constants and dielectric loss of 1788PVA and 10T@1788PVA films at different frequency were shown in Figure 2A2 and 2B2. The dielectric constants of the 1788PVA and 10T@1788PVA films both increased with temperature. The values for 10T@1788PVA were consistently higher than those for 1788PVA and the differences further increased under high temperatures and low frequency. This result indicated the enhancement of charges storage ability by incorporating TEDA.C, which was implied from the significant increase of dielectric constant.[52] In Figure 2B2, the peaks of dielectric loss for 10T@1788PVA shifted to low temperature, which was attributed to the α_a-relaxation of PVA, during which the micro-Brownian motion of long chain segments in the amorphous regions of PVA took place.[43,44] The peak of 1788PVA appeared at 375 K and was attributed to the α_c-relaxation.[53,54] This peak was above the T_g tested by DMA (Figure 4C), which was due to the segmental motion in the 1788PVA crystalline phase.[44] For 10 and 100 Hz frequency, the dielectric loss of 10T@1788PVA was higher than that of 1788PVA. For 1788PVA, as the covalent bond rotated under cyclic electric field, the existing flexible polar groups with polar bonds caused dielectric-transition. Thus, embedding the TEDA.C crystallite within the PVA chains facilitated the segmental motion and decreased 1788PVA crystalline phase, which in turn lead to more flexible polymer chains and, hence, enhanced the tan δ.[41,55] Both temperature- and frequency-dependent dielectric properties of the 1788PVA and 10T@1788PVA films were shown in Figure 2A3, 2A4, 2B3, and 2B4. The 10T@1788PVA showed a rapid increase of dielectric constant with the addition of TEDA.C, as well as the interaction between TEDA.C and PVA chains.

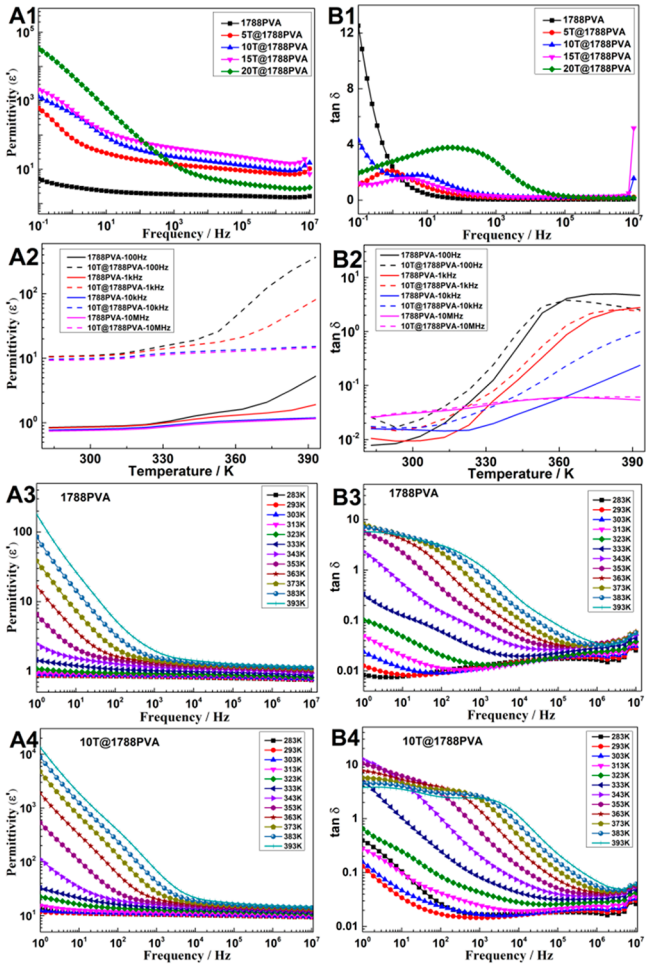

Figure 2. Frequency dependence of (A1) the dielectric constant at 0.1 Hz−10 MHz at room temperature and (B1) the dielectric loss at 0.1 Hz−10 MHz at room temperature. Temperature dependence of (A2) the dielectric constant at 100 Hz, 1 kHz, 10 kHz, and 10 MHz and (B2) the dielectric loss at 100 Hz, 1 kHz, 10 kHz, and 10 MHz. Both temperature frequency dependence of (A3, A4) dielectric constant and (B3, B4) the dielectric loss of 1788PVA and PVA composites films.

The polarization-electric loops (P-E loops) of 1788PVA and 10T@1788PVA were tested under different electric fields at 1000 Hz (Figure 3). 10T@1788PVA films displayed increased saturation polarization in comparison to that of neat PVA film. In this study, the remnant polarization of composites was 0.779μC/cm^2 at 60 MV/m, whereas that of the neat PVA film was around 0.000243 μC/cm^2 at 60 MV/m. The coercive field

https://dx.doi.org/10.1021/acsmaterialslett.0c00086
ACS Materials Lett. 2020, 2, 453−460

Table 1. Increase of the Dielectric Constants in Different Systems

samples	polymer	fills	additive amount	dielectric constant	increment	refs
1	PDMS[a]	M-CCTO[b]	2 wt %	~14	38% at 10 Hz	20
2	PVDF-HFP[c]	BT-NPs[d]	10 vol %	~9.6	67% at 0.01 Hz	6
3	PVDF-HFP[c]	BT-NWs[e]	10 vol %	~104	300 times at 0.01 Hz	6
4	PVDF-HFP[c]	BT[f]	70 vol %	~38	2 times at 100 Hz	7
5	PVDF[g]	Mg-salt[h]	2 wt %	~35	2.5 times at 1000 Hz	51
6	PVDF[g]	PI@BT[i]	40 wt %	~148	7.4 times at 10 Hz	62
7	ABS[j]	MWCNT[k]	7 wt %	~400	100 times at 100 Hz	21
8	ABS[j]	GCNT[l]	10 wt %	~85	40 times at 100 Hz	21
9	P(VDF-TrFE-CFE)[m]	BNNS[n]	25 wt %	~55	15% at 100 Hz	32
10	epoxy	F-MWCNT[o]	8 wt %	~60	11.9 times at 100 Hz	17
11	PMMA/P(VDF-HFP)	DOPA@TiO_2[p]	20 wt %	~13	1.24 times at 100 Hz	63
12	PVA	CuI	7.5 wt %	~1000	2.5 times at 100 Hz	55
13	PVA	TEDA.C	4.7 wt %	30	12.7 times at 10 Hz	this work
14	PVA	TEDA.C	16 wt %	610	285.36 times at 10 Hz	this work
15	PVA	TEDA.C	9 wt %	24486	943 times at 10 Hz at 383 K	this work
16	PVA	TEDA.C	9 wt %	15.6	9.5 times at 10^7 Hz	this work

[a]Polydimethyl siloxane. [b]Magnesium-doped calcium copper titanate. [c]Poly(vinylidene fluoridetrifluoroethylene). [d]$BaTiO_3$ nanoparticles. [e]$BaTiO_3$ nanowires. [f]$BaTiO_3$. [g]Polyvinylidene fluoride. [h]$MgCl_2{\cdot}6H_2O$. [i]Polyimide (PI) interlayer with nanoscale thickness was coated on the surface of barium titanate ($BaTiO_3$, BT) through the in-situ polymerization and subsequent thermal imidization treatment. [j]Acrylonitrile−butadiene−styrene. [k]Multiwalled carbon nanotube. [l]Graphene oxide-carbon nanotube. [m]Poly(vinylidene fluoride-trifluoroethylene-chlorofluoroethylene) terpolymer. [n]Boron nitride nanosheets. [o]Fluorinated MWCNTs. [p]Polydopamine-coated TiO_2.

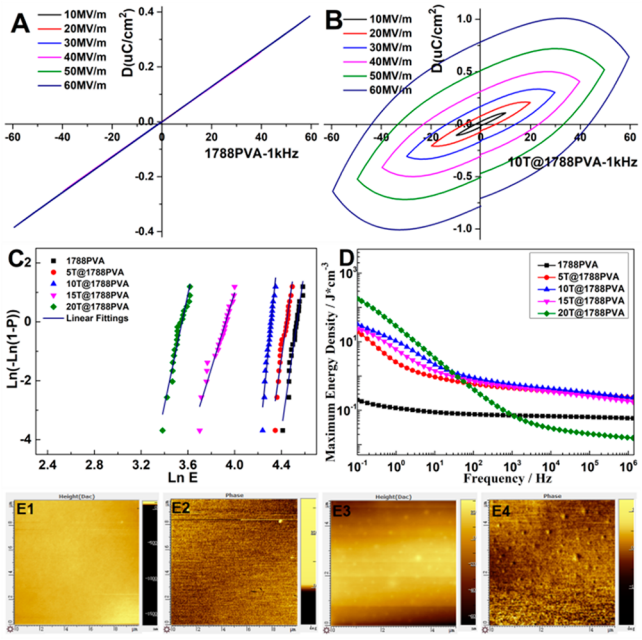

Figure 3. Hysteresis loops at 1000 Hz under different electric fields for (A) 1788PVA films and (B) 10T@1788PVA. (C) Weibull distribution curves of PVA composites with different content of TEDA.C at room temperature under AC electric field. (D) Dependency of frequency for the calculated maximum energy storage density of the TEDA.C@PVA films at room temperature under AC electric field. (E1) AFM topographic image of 1788PVA, (E2) AFM phase image of 1788PVA, (E3) AFM topographic image of 10T@1788PVA, and (E4) AFM phase image of 10T@1788PVA.

of PVA composite films was increased by about 941.7 times with 9 wt.% TEDA.C. According to the Weibull distribution curves (Figure 3C), the breakdown strength (Eb) under AC electric field of each films was calculated (Table 2). With low TEDA.C addition, the breakdown strength of PVA composite films decreased slowly. But the decrease in the breakdown strength of PVA composites films with 13 wt.% and 16 wt.%

Table 2. Weibull Parameters and Electrical Breakdown Strength of PVA and PVA Composite Films

samples	intercept	slope	E_0[a] (MV/m)
1788PVA	−124.11	27.38	92.76
5T@1788PVA	−123.15	27.71	84.77
10T@1788PVA	−170.74	39.59	74.44
15T@1788PVA	−50.70	12.92	50.40
20T@1788PVA	−66.73	18.80	34.81

[a]Dielectric strength was tested under AC electric field

TEDA.C were bigger. This should be due to the TEDA.C dendritic crystal network within PVA matrix. According to the calculated breakdown field strength and dielectric constant, we calculated maximum energy storage density of the TEDA.C@PVA films (Figure 3D). For 1788PVA, the maximum energy storage density was 0.06−0.20 J/cm^3, increasing with the decreasing frequency. When the frequency was 1 kHz, the maximum energy storage density of 5T@1788PVA, 10T@1788PVA, and 15T@1788PVA was 6.15×, 7.96×, and 6.53× of 1788PVA. The surface morphology and distribution of the TEDA.C in PVA films were characterized by AFM. 10T@1788PVA showed increased surface roughness due to the crystallization of TEDA.C (further confirmed by POM and AFM in Figures S6 and S7) and uniform phase dispersion of TEDA.C in 1788PVA (Figure 3E). Interestingly, the phase degree of the composite film was not increased, implying that no phase separation occurred on the surface of film and that the TEDA.C crystals were inside the film. These results suggested that PVA can form a good protective layer over the TEDA.C crystals by hydrogen bonding at the interfaces between TEDA.C and PVA interface.

Composites films with adjustable transmittance and good flexibility were also highly desirable in the design of flexible electronics.[56−58] The PVA/TEDA.C composite films with 4.7 and 9 wt % TEDA.C maintained ultrahigh transmittance throughout the visible range (Figure 4A, the photo of films was in Figure S24). The formation of uniform transparent film is

https://dx.doi.org/10.1021/acsmaterialslett.0c00086
ACS Materials Lett. 2020, 2, 453−460

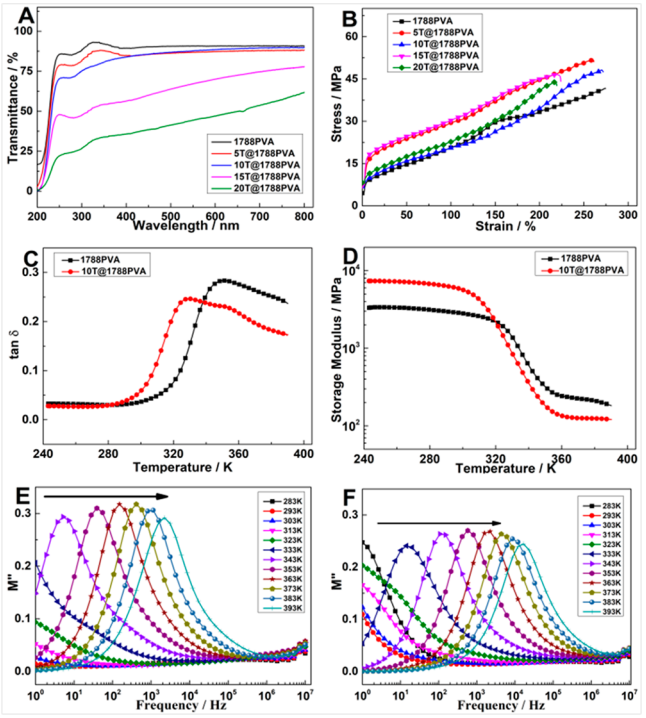

Figure 4. (A) Light transmittance of TEDA.C@1788PVA composite films with different TEDA.C loadings. (B) Stress−strain curves of 1788PVA and TEDA.C@1788PVA composite films. (C) tan δ curves of 1788PVA and 10T@1788PVA composite films by DMA test. (D) Storage modulus curves of 1788PVA and 10T@1788PVA composite films by DMA test. (E) Dielectric modulus of 1788PVA at 1 Hz−10 MHz under different temperature. (F) Dielectric modulus of 10T@1788PVA at 1 Hz−10 MHz under different temperature.

due to the similar solubility of TEDA.C and PVA that facilitate obtaining homogeneous and transparent solution. The good optical transparency of the composite film enabled its potential applications for stretchable and transparent actuators,[59] touch panel,[60] and electric skin.[61] For the mechanical properties (Figure 4B), the 5T@1788PVA and 10T@1788PVA composites films exhibited fracture strain as high as 274%, which is almost the same as the PVA only films, suggesting the excellent TEDA.C distribution in the film. Notably, films containing 16 wt % TEDA.C can still maintain the elongation at break around 222%. Meanwhile, the tensile strength was increased from 41.7 to 51.7 MPa with addition of 4.7 wt % TEDA.C. When the TEDA.C was further increased to 20 wt %, the tensile strength of the film decreased to 43.7 MPa, but it was still higher than that of pure 1788PVA. Meanwhile, the thermal stability of composites films was also studied by thermal gravimetric analyzer (TGA). The results showed the excellent dispersion of TEDA.C in PVA material did not impair the thermal stability of PVA (in Figure S25).

Figure 4C showed the temperature dependence of the tan δ for PVA and TEDA.C-incorporated PVA films. The peak of tan δ curve for 10T@1788PVA shifted to lower temperature. Figure 4D showed the tensile storage modulus at 1 Hz as a function of temperature for PVA films and TEDA.C composite films. Below the T_g of PVA, there was a noticeable increase in modulus for both films because of the restricted chain mobility. The modulus for the 10T@1788PVA film increased for 116%, compared to the 1788PVA at 260 K. But above the T_g of PVA, there was great reduction in the modulus. The dielectric modulus showed the segment relaxation under AC electric field (Figure 4E and 4F). With the addition of TEDA.C, the peaks of dielectric modulus shifted to high frequencies and decreased to low values, confirming the interaction of TEDA.C, and PVA chains decreased the T_g of PVA. For example, the storage modulus for 10T@1788PVA film decreased by 44% at 370 K, yet still higher than that of PVA films.

In this work, we synthesized and demonstrated a flexible and transparent TEDA.C/PVA composite film with significantly enhanced dielectric constant by hydrogen bond interaction. The dielectric constant can be increased by 10−50 times with low addition of TEDA.C. This remarkable performance was contributed by the ultrafast polarization switching of TEDA.C in AC electric field and interfacial interaction. The enhancement of the stretching vibration of −OH groups in composite film by ATR tests and the absorbance strength of −OH groups for 5T@1788PVA under AC electric field suggested that the dipole moment of hydrogen bonds formed by the accumulation of charges at the interfaces between TEDA.C crystals and polymer backbones contribute to the improvement of dielectric constant in this system. According to the Weibull distribution law, the breakdown strength of PVA composite films decreased slowly with low addition of TEDA.C. However, the increasing dielectric constant improved the maximum energy storage density of PVA composites. The calculated maximum energy storage density of 10T@1788PVA was 10.7× of that of 1788PVA at 100 Hz. The results of P-E loops indicated that the remnant polarization of PVA composite films increased by 3200 times with 9 wt % TEDA.C, which suggested that TEDA.C significantly increased the ferroelectric property of 1788PVA. The AFM and POM characterizations implied the TEDA.C crystals were uniformly dispersed in PVA matrix. With the increase of TEDA.C, rod-like structure of TEDA.C crystals gradually changed to crosslinked morphology at >9 wt % TEDA.C concentration. The tan δ of 10T@1788PVA slightly shifted to lower temperatures with a 116% increase of the storage modulus, compared to 1788PVA at 260 K in DMA mode. PVA films kept transparent and flexible with 4.7 and 9 wt % addition of TEDA.C, providing attractive materials for stretchable and transparent actuators, touch panel and electric skin. In addition, the high dielectric constant, stretchability, low Young's modulus and easily control processing of PVA composite films facilitate TEDA.C@PVA composites for multifunctional electroactive films for soft-robotics, optics, and microfluidics.

■ ASSOCIATED CONTENT

Supporting Information

The Supporting Information is available free of charge at https://pubs.acs.org/doi/10.1021/acsmaterialslett.0c00086.

Details of materials and methods, sample preparation of films, characterization of TEDA.C, and dielectric properties of PVA composite films, polypropylene composites films, and polyvinylidene fluoride composites films (PDF)

■ AUTHOR INFORMATION

Corresponding Authors

Xufu Cai − *College of Polymer Science and Materials, The State Key Laboratory of Polymer Materials Engineering, Sichuan*

https://dx.doi.org/10.1021/acsmaterialslett.0c00086
ACS Materials Lett. 2020, 2, 453−460

University, Chengdu 610065, China; orcid.org/0000-0003-4501-7634; Email: caixf2008@scu.edu.cn

Ximin He − *Department of Materials Science and Engineering, University of California Los Angeles, Los Angeles, California 90024, United States;* orcid.org/0000-0001-8845-4637; Email: ximinhe@ucla.edu

Authors

Yunyun Yang − *College of Polymer Science and Materials, The State Key Laboratory of Polymer Materials Engineering, Sichuan University, Chengdu 610065, China; Department of Materials Science and Engineering, University of California Los Angeles, Los Angeles, California 90024, United States*

Yusen Zhao − *Department of Materials Science and Engineering, University of California Los Angeles, Los Angeles, California 90024, United States*

Jun Liu − *College of Chemistry and Environment Protection Engineering, Southwest Minzu University, Chengdu 610041, China*

Zekun Nie − *College of Polymer Science and Materials, The State Key Laboratory of Polymer Materials Engineering, Sichuan University, Chengdu 610065, China*

Jun Ma − *College of Polymer Science and Materials, The State Key Laboratory of Polymer Materials Engineering, Sichuan University, Chengdu 610065, China*

Mutian Hua − *Department of Materials Science and Engineering, University of California Los Angeles, Los Angeles, California 90024, United States*

Yucheng Zhang − *Department of Materials Science and Engineering, University of California Los Angeles, Los Angeles, California 90024, United States*

Complete contact information is available at: https://pubs.acs.org/10.1021/acsmaterialslett.0c00086

Author Contributions

‡Y.Y. and Y.Z. contributed equally to this work.

Funding

This work was financially supported by the National Natural Science Foundation of China (NSFC 51873114), the China Scholarship Council (CSC 201806240114), the Hellman Fellows Funds, the AFOSR Grant FA9550-17-1-0311, the AFOSR award FA9550-18-1-0449, the ONR Award N000141712117, and the ONR Award N00014-18-1-2314.

Notes

The authors declare no competing financial interest.

■ ACKNOWLEDGMENTS

The authors thank Gehong Su and Prof. Tao Zhou from the State Key Laboratory of Polymer Materials Engineering, Sichuan University, for their 2D-FTIR tests and suggestions.

■ ABBREVIATIONS

TEDA.C, $[Hdabco]ClO_4$ (dabco = diazabicyclo[2.2.2]octane); PVA, poly(vinyl alcohol); PP, polypropylene; PVDF, polyvinylidene fluoride; BTO, barium titanate; PZT, lead zirconate titanate; AFM, atomic force microscopy; POM, polarizing microscope; MWS, Maxwell−Wagner−Sillars

■ REFERENCES

(1) Bentsen, N. S.; Møller, I. M. Solar energy conserved in biomass: Sustainable bioenergy use and reduction of land use change. *Renewable Sustainable Energy Rev.* **2017**, *71*, 954−958.

(2) Cassettari, L.; Bendato, I.; Mosca, M.; Mosca, R. Energy Resources Intelligent Management using on line real-time simulation: A decision support tool for sustainable manufacturing. *Appl. Energy* **2017**, *190*, 841−851.

(3) Ziemele, J.; Gravelsins, A.; Blumberga, A.; Blumberga, D. Sustainability of heat energy tariff in district heating system: Statistic and dynamic methodologies. *Energy* **2017**, *137*, 834−845.

(4) Centobelli, P.; Cerchione, R.; Esposito, E. Environmental Sustainability and Energy-Efficient Supply Chain Management: A Review of Research Trends and Proposed Guidelines. *Energies* **2018**, *11*, 275.

(5) Wang, H.; Xie, H.; Wang, S.; Gao, Z.; Li, C.; Hu, G.-H.; Xiong, C. Enhanced dielectric property and energy storage density of PVDF-HFP based dielectric composites by incorporation of silver nanoparticles-decorated exfoliated montmorillonite nanoplatelets. *Composites, Part A* **2018**, *108*, 62−68.

(6) Feng, Y.; Li, W. L.; Hou, Y. F.; Yu, Y.; Cao, W. P.; Zhang, T. D.; Fei, W. D. Enhanced dielectric properties of PVDF-HFP/$BaTiO_3$-nanowire composites induced by interfacial polarization and wire-shape. *J. Mater. Chem. C* **2015**, *3*, 1250−1260.

(7) Hao, Y.; Wang, X.; Bi, K.; Zhang, J.; Huang, Y.; Wu, L.; Zhao, P.; Xu, K.; Lei, M.; Li, L. Significantly enhanced energy storage performance promoted by ultimate sized ferroelectric $BaTiO_3$ fillers in nanocomposite films. *Nano Energy* **2017**, *31*, 49−56.

(8) Dai, Z.-H.; Li, T.; Gao, Y.; Xu, J.; Weng, Y.; He, J.; Guo, B.-H. Improved dielectric and energy storage properties of poly(vinyl alcohol) nanocomposites by strengthening interfacial hydrogen-bonding interaction. *Colloids Surf., A* **2018**, *548*, 179−190.

(9) Dang, Z. M.; Zheng, M. S.; Zha, J. W. 1D/2D Carbon Nanomaterial-Polymer Dielectric Composites with High Permittivity for Power Energy Storage Applications. *Small* **2016**, *12*, 1688−701.

(10) Brown, L. J.; Dickerson, S. A.; Curry, R. D.; Mounter, S. A.; Mcfarland, J. A. Characterization of the temperature dependence of the electrical and mechanical properties of a high breakdown strength nanodielectric composite. *IEEE Trans. Dielectr. Electr. Insul.* **2019**, *26*, 455−460.

(11) Anderson, I. A.; Gisby, T. A.; Mckay, T. G.; O'Brien, B. M.; Calius, E. P. Multi-functional dielectric elastomer artificial muscles for soft and smart machines. *J. Appl. Phys.* **2012**, *112*, 041101−041101-20.

(12) Araromi, O. A.; Gavrilovich, I.; Shintake, J.; Rosset, S.; Richard, M.; Gass, V.; Shea, H. R. Rollable Multisegment Dielectric Elastomer Minimum Energy Structures for a Deployable Microsatellite Gripper. *IEEE/ASME Transactions on Mechatronics* **2015**, *20*, 438−446.

(13) Murray, C.; McCoul, D.; Sollier, E.; Ruggiero, T.; Niu, X.; Pei, Q.; Di Carlo, D. Dino, Electro-adaptive microfluidics for active tuning of channel geometry;using polymer actuators. *Microfluid. Nanofluid.* **2013**, *14*, 345−358.

(14) O'Halloran, A.; O'malley, F.; McHugh, P. A review on dielectric elastomer actuators, technology, applications, and challenges. *J. Appl. Phys.* **2008**, *104*, 071101.

(15) Shian, S.; Diebold, R. M.; Clarke, D. R. Tunable lenses using transparent dielectric elastomer actuators. *Opt. Express* **2013**, *21*, 8669−8676.

(16) Gao, H.; Li, J.; Zhang, F.; Liu, Y.; Leng, J. The research status and challenges of shape memory polymers in flexible electronics and structural devices. *Mater. Horiz.* **2019**, *6*, 931.

(17) Liu, Y.; Zhang, C.; Huang, B.; Wang, X.; Li, Y.; Wang, Z.; Lai, W.; Zhang, X.; Liu, X. Skin-core structured fluorinated MWCNTs: a nanofiller towards a broadband dielectric material with a high dielectric constant and low dielectric loss. *J. Mater. Chem. C* **2018**, *6*, 2370−2378.

(18) Tu, S.; Jiang, Q.; Zhang, X.; Alshareef, H. N. Large Dielectric Constant Enhancement in MXene Percolative Polymer Composites. *ACS Nano* **2018**, *12*, 3369−3377.

(19) Ye, H.; Lu, T.; Xu, C.; Zhong, M.; Xu, L. Enhanced energy density and thermal conductivity in poly(fluorovinylidene-co-hexafluoropropylene) nanocomposites incorporated with boron

nitride nanosheets exfoliated under assistance of hyperbranched polyethylene. *Nanotechnology* **2018**, *29*, 095702.
(20) Duan, L.; Wang, G. L.; Zhang, Y. Y.; Zhang, Y. N.; Wei, Y. Y.; Wang, Z. F.; Zhang, M. High dielectric and actuated properties of silicone dielectric elastomers filled with magnesium-doped calcium copper titanate particles. *Polym. Compos.* **2018**, *39*, 691−697.
(21) Jyoti, J.; Kumar, A.; Dhakate, S. R.; Singh, B. P. Dielectric and impedance properties of three dimension graphene oxide-carbon nanotube acrylonitrile butadiene styrene hybrid composites. *Polym. Test.* **2018**, *68*, 456−466.
(22) Liu, Z.; Paterson, A. R.; Wu, H.; Gao, P.; Ren, W.; Ye, Z.-G. Synthesis, structure and piezo-/ferroelectric properties of a novel bismuth-containing ternary complex perovskite solid solution. *J. Mater. Chem. C* **2017**, *5*, 3916−3923.
(23) Daneshpajooh, H.; Shekhani, H. N.; Choi, M.; Uchino, K. New methodology for determining the dielectric constant of a piezoelectric material at the resonance frequency range. *J. Am. Ceram. Soc.* **2018**, *101*, 1940−1948.
(24) Marwat, M. A.; Xie, B.; Ashtar, M.; Zhu, Y.; Fan, P.; Zhang, H. High remnant polarization, high dielectric constant and impedance performance of Nb/In Co-doped $Bi_{0.49}La_{0.01}Na_{0.49}$ $Li_{0.01}TiO_3$-δ ceramics. *Ceram. Int.* **2018**, *44*, 6843−6850.
(25) Sanches, A. O.; Kanda, D. H. F.; Malmonge, L. F.; da Silva, M. J.; Sakamoto, W. K.; Malmonge, J. A. Synergistic effects on polyurethane/lead zirconate titanate/carbon black three-phase composites. *Polym. Test.* **2017**, *60*, 253−259.
(26) Valiyaneerilakkal, U.; Singh, A.; Subash, C. K.; Singh, K.; Abbas, S. M.; Varghese, S. Preparation and characterization of poly(vinylidene fluoride-trifluoroethylene)/barium titanate polymer nanocomposite for ferroelectric applications. *Polym. Compos.* **2017**, *38*, 1655−1661.
(27) Chaisan, W.; Yimnirun, R.; Ananta, S.; Cann, D. P. Dielectric properties of solid solutions in the lead zirconate titanate-barium titanate system prepared by a modified mixed-oxide method. *Mater. Lett.* **2005**, *59*, 3732−3737.
(28) Ji, S.; Jang, J.; Cho, E.; Kim, S. H.; Kang, E. S.; Kim, J.; Kim, H. K.; Kong, H.; Kim, S. K.; Kim, J. Y.; Park, J. U. High Dielectric Performances of Flexible and Transparent Cellulose Hybrid Films Controlled by Multidimensional Metal Nanostructures. *Adv. Mater.* **2017**, *29*, 1700538.
(29) Hammock, M. L.; Chortos, A.; Tee, B. C.; Tok, J. B.; Bao, Z. 25th anniversary article: The evolution of electronic skin (e-skin): a brief history, design considerations, and recent progress. *Adv. Mater.* **2013**, *25*, 5997−6038.
(30) Lee, M.; Chen, C. Y.; Wang, S.; Cha, S. N.; Park, Y. J.; Kim, J. M.; Chou, L. J.; Wang, Z. L. A hybrid piezoelectric structure for wearable nanogenerators. *Adv. Mater.* **2012**, *24*, 1759−64.
(31) Lin, L.; Hu, Y.; Xu, C.; Zhang, Y.; Zhang, R.; Wen, X.; Lin Wang, Z. Transparent flexible nanogenerator as self-powered sensor for transportation monitoring. *Nano Energy* **2013**, *2*, 75−81.
(32) Liu, F.; Li, Q.; Li, Z.; Dong, L.; Xiong, C.; Wang, Q. Ternary PVDF-based terpolymer nanocomposites with enhanced energy density and high power density. *Composites, Part A* **2018**, *109*, 597−603.
(33) Briscoe, J.; Jalali, N.; Woolliams, P.; Stewart, M.; Weaver, P. M.; Cain, M.; Dunn, S. Measurement techniques for piezoelectric nanogenerators. *Energy Environ. Sci.* **2013**, *6*, 3035.
(34) Horiuchi, S.; Tsutsumi, J. y.; Kobayashi, K.; Kumai, R.; Ishibashi, S. Piezoelectricity of strongly polarized ferroelectrics in prototropic organic crystals. *J. Mater. Chem. C* **2018**, *6*, 4714−4719.
(35) Horiuchi, S.; Tokunaga, Y.; Giovannetti, G.; Picozzi, S.; Itoh, H.; Shimano, R.; Kumai, R.; Tokura, Y. Erratum: Above-room-temperature ferroelectricity in a single-component molecular crystal. *Nature* **2010**, *466*, 1006−1006.
(36) Fu, D.-W.; Cai, H.-L.; Liu, Y.; Ye, Q.; Zhang, W.; Zhang, Y.; Chen, X.-Y.; Giovannetti, G.; Capone, M.; Li, J.; Xiong, R.-G. Diisopropylammonium bromide is a high-temperature molecular ferroelectric crystal. *Science* **2013**, *339*, 425.
(37) Tang, Y. Y.; Zhang, W. Y.; Li, P. F.; Ye, H. Y.; You, Y. M.; Xiong, R. G. Ultrafast Polarization Switching in a Biaxial Molecular Ferroelectric Thin Film: [Hdabco]ClO_4. *J. Am. Chem. Soc.* **2016**, *138*, 15784−15789.
(38) Subba Reddy, C. V.; Han, X.; Zhu, Q.-Y.; Mai, L.-Q.; Chen, W. Dielectric spectroscopy studies on (PVP+PVA) polyblend film. *Microelectron. Eng.* **2006**, *83*, 281−285.
(39) Deshmukh, K.; Ahamed, M. B.; Deshmukh, R. R.; Khadheer Pasha, S. K.; Sadasivuni, K. K.; Ponnamma, D.; Chidambaram, K. Synergistic effect of vanadium pentoxide and graphene oxide in polyvinyl alcohol for energy storage application. *Eur. Polym. J.* **2016**, *76*, 14−27.
(40) Mahendia, S.; Tomar, A. K.; Kumar, S. Electrical conductivity and dielectric spectroscopic studies of PVA-Ag nanocomposite films. *J. Alloys Compd.* **2010**, *508*, 406−411.
(41) Bhajantri, R. F.; Ravindrachary, V.; Harisha, A.; Ranganathaiah, C.; Kumaraswamy, G. N. Effect of barium chloride doping on PVA microstructure: positron annihilation study. *Appl. Phys. A: Mater. Sci. Process.* **2007**, *87*, 797−805.
(42) Enayati, M. S.; Behzad, T.; Sajkiewicz, P. Ł.; Bagheri, R.; Ghasemi-Mobarakeh, L.; Pierini, F. Theoretical and experimental study of the stiffness of electrospun composites of poly(vinyl alcohol), cellulose nanofibers, and nanohydroxy apatite. *Cellulose* **2018**, *25*, 65−75.
(43) El Sayed, A. M. Synthesis and controlling the optical and dielectric properties of CMC/PVA blend via γ-rays irradiation. *Nucl. Instrum. Methods Phys. Res., Sect. B* **2014**, *321*, 41−48.
(44) Abdel-Baset, T. A.; Hassen, A. Dielectric relaxation analysis and Ac conductivity of polyvinyl alcohol/polyacrylonitrile film. *Phys. B* **2016**, *499*, 24−28.
(45) Barandiaran, I.; Gutierrez, J.; Etxeberria, H.; Tercjak, A.; Kortaberria, G. Tuning photoresponsive and dielectric properties of PVA/CdSe films by capping agent change. *Composites, Part A* **2019**, *118*, 194−201.
(46) Irfan, M.; Razikha Banu, S.; Sahana Kumari, R.; Veena, B. M.; Madhu, B. J.; Manjunath, A. Preparation, structural characterization and electrical studies on NiO doped PVA films. *Materials Today: Proceedings* **2018**, *5*, 10839−10844.
(47) Ishaq, S.; Kanwal, F.; Atiq, S.; Moussa, M.; Azhar, U.; Gul, I.; Losic, D. Dielectric and impedance spectroscopic studies of three phase graphene/titania/poly(vinyl alcohol) nanocomposite films. *Results Phys.* **2018**, *11*, 540−548.
(48) Kandhol, G.; Wadhwa, H.; Chand, S.; Mahendia, S.; Kumar, S. Study of dielectric relaxation behavior of composites of Poly (vinyl alchohol) (PVA) and Reduced graphene oxide (RGO). *Vacuum* **2019**, *160*, 384−393.
(49) Thakur, P.; Kool, A.; Bagchi, B.; Hoque, N. A.; Das, S.; Nandy, P. In situ synthesis of $Ni(OH)_2$ nanobelt modified electroactive poly(vinylidene fluoride) thin films: remarkable improvement in dielectric properties. *Phys. Chem. Chem. Phys.* **2015**, *17*, 13082−91.
(50) Thakur, P.; Kool, A.; Bagchi, B.; Das, S.; Nandy, P. Effect of in situ synthesized Fe_2O_3 and Co_3O_4 nanoparticles on electroactive beta phase crystallization and dielectric properties of poly(vinylidene fluoride) thin films. *Phys. Chem. Chem. Phys.* **2015**, *17*, 1368−78.
(51) Jana, S.; Garain, S.; Sen, S.; Mandal, D. The influence of hydrogen bonding on the dielectric constant and the piezoelectric energy harvesting performance of hydrated metal salt mediated PVDF films. *Phys. Chem. Chem. Phys.* **2015**, *17*, 17429−36.
(52) Yang, Y.; Li, Z.; Ji, W.; Sun, C.; Deng, H.; Fu, Q. Enhanced dielectric properties through using mixed fillers consisting of nano-barium titanate/nickel hydroxide for polyvinylidene fluoride based composites. *Composites, Part A* **2018**, *104*, 24−31.
(53) Hdidar, M.; Chouikhi, S.; Fattoum, A.; Arous, M. Effect of hydrolysis degree and mass molecular weight on the structure and properties of PVA films. *Ionics* **2017**, *23*, 3125−3135.
(54) Gun'ko, V. M.; Pissis, P.; Spanoudaki, A.; Zarko, V. I.; Nychiporuk, Y. M.; Andriyko, L. S.; Goncharuk, E. V.; Leboda, R.; Skubiszewska-Zieba, J.; Osovskii, V. D.; Ptushinskii, Y. G. Relaxation

https://dx.doi.org/10.1021/acsmaterialslett.0c00086
ACS Materials Lett. 2020, 2, 453−460

phenomena in poly(vinyl alcohol)/fumed silica affected by interfacial water. *J. Colloid Interface Sci.* **2007**, *312*, 201−13.
(55) Mohamed, S. A.; Al-Ghamdi, A. A.; Sharma, G. D.; El Mansy, M. K. Effect of ethylene carbonate as a plasticizer on CuI/PVA nanocomposite: Structure, optical and electrical properties. *J. Adv. Res.* **2014**, *5*, 79−86.
(56) Kim, S.-W.; Kim, K.; Nah, W.; Lee, C.-R.; Jung, S.-B.; Kim, J.-W. Transparent and flexible high frequency transmission lines based on composite structure comprising silver nanowires and polyvinyl butyral. *Compos. Sci. Technol.* **2018**, *159*, 25−32.
(57) Trung, T. Q.; Ramasundaram, S.; Hwang, B. U.; Lee, N. E. An All-Elastomeric Transparent and Stretchable Temperature Sensor for Body-Attachable Wearable Electronics. *Adv. Mater.* **2016**, *28*, 502−9.
(58) You, B.; Kim, Y.; Ju, B. K.; Kim, J. W. Highly Stretchable and Waterproof Electroluminescence Device Based on Superstable Stretchable Transparent Electrode. *ACS Appl. Mater. Interfaces* **2017**, *9*, 5486−5494.
(59) Keplinger, C.; Sun, J.-Y.; Foo, C. C.; Rothemund, P.; Whitesides, G. M.; Suo, Z. Stretchable, Transparent, Ionic Conductors. *Science* **2013**, *341*, 984−987.
(60) Kim, C.-C.; Lee, H.-H.; Oh, K. H.; Sun, J.-Y. Highly stretchable, transparent ionic touch panel. *Science* **2016**, *353*, 682−687.
(61) Pu, X.; Guo, H.; Chen, J.; Wang, X.; Xi, Y.; Hu, C.; Wang, Z. L. Ultrastretchable, transparent triboelectric nanogenerator as electronic skin for biomechanical energy harvesting and tactile sensing. *Science Advances* **2017**, *3*, e1700694.
(62) Xie, X.; Yang, C.; Qi, X.-d.; Yang, J.-h.; Zhou, Z.-w.; Wang, Y. Constructing polymeric interlayer with dual effects toward high dielectric constant and low dielectric loss. *Chem. Eng. J.* **2019**, *366*, 378−389.
(63) Zhu, Y.; Yao, H.; Jiang, P.; Wu, J.; Zhu, X.; Huang, X. Two-Dimensional High-k Nanosheets for Dielectric Polymer Nanocomposites with Ultrahigh Discharged Energy Density. *J. Phys. Chem. C* **2018**, *122*, 18282−18293.

https://dx.doi.org/10.1021/acsmaterialslett.0c00086
ACS Materials Lett. 2020, 2, 453−460